Science Advances
AAAS

Supplementary Materials for

The role of ipRGCs in ocular growth and myopia development

Ai-Lin Liu *et al.*

Corresponding author: Xiong-Li Yang, xlyang@fudan.edu.cn; Shi-Jun Weng, sjweng@fudan.edu.cn; Yong-Mei Zhong, ymzhong@fudan.edu.cn

Sci. Adv. **8**, eabm9027 (2022)
DOI: 10.1126/sciadv.abm9027

This PDF file includes:

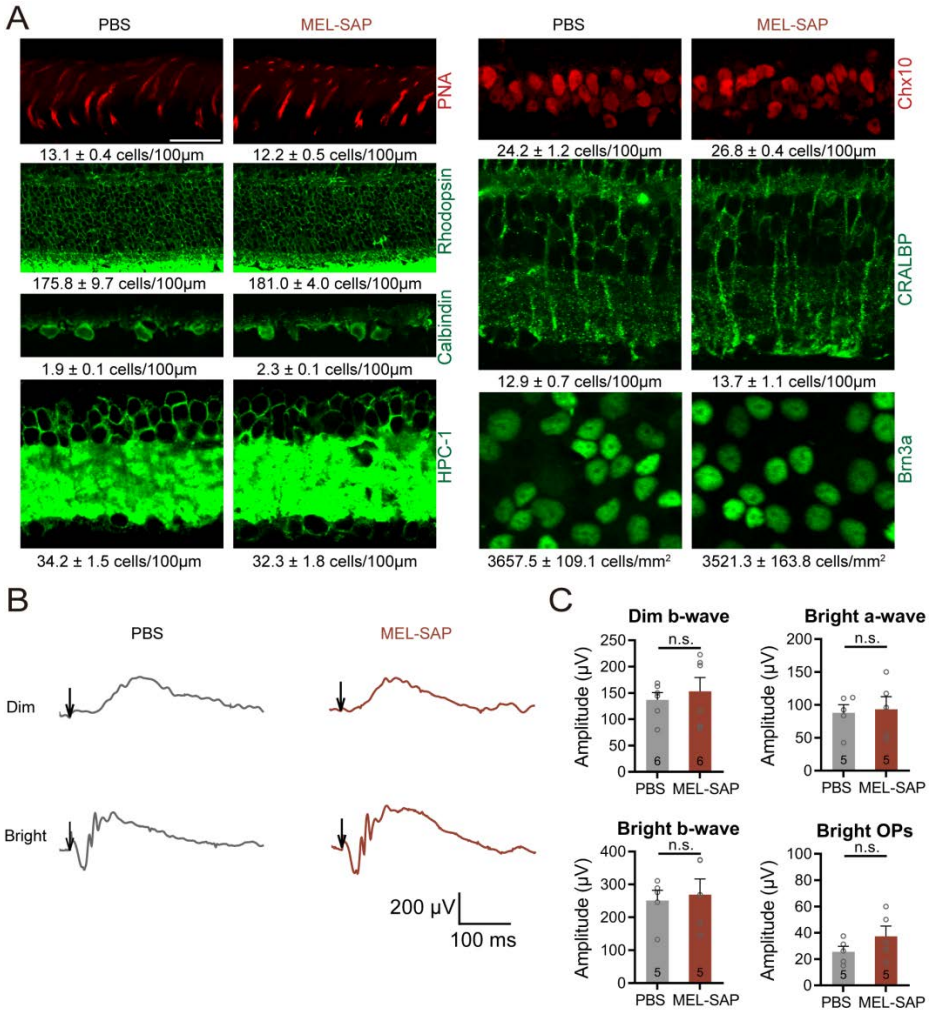

Fig. S1. MEL-SAP does not cause loss of non-ipRGC cells or change overall physiological functions of the retina. (A) Representative confocal images of C57BL/6 retinal sections/whole mounts captured at D14, showing immunostaining of various molecular markers for retinal cells, including PNA (cone), rhodopsin (rod), calbindin (horizontal cell), HPC-1 (amacrine cell), Chx10 (ON bipolar cell), CRALBP (Müller cell) and Brn3a (conventional GCs). None of these cell types showed significantly different densities (listed beneath each panel) between 400 ng MEL-SAP- and PBS-injected eyes. All n = 3. Scale bar, 20 μm. **(B)** Representative dark-adapted ERGs recorded from 400 ng MEL-SAP- and PBS-injected eyes at D14. ERGs were evoked by dim (0.01 cd/cm^2·s) and bright (3 cd/cm^2·s) flashes (3 ms, arrows) to evaluate rod-dominant and mixed rod-cone responses, respectively. **(C)** Bar charts comparing average ERG amplitudes between 400 ng MEL-SAP- and PBS-injected eyes. For all four sets of parameters analyzed (b-waves elicited by dim flashes and a-, b-waves and oscillatory potentials [Ops] elicited by bright flashes), no significant difference was found between the two eyes. Error bars represent SEM. n.s. not significant.

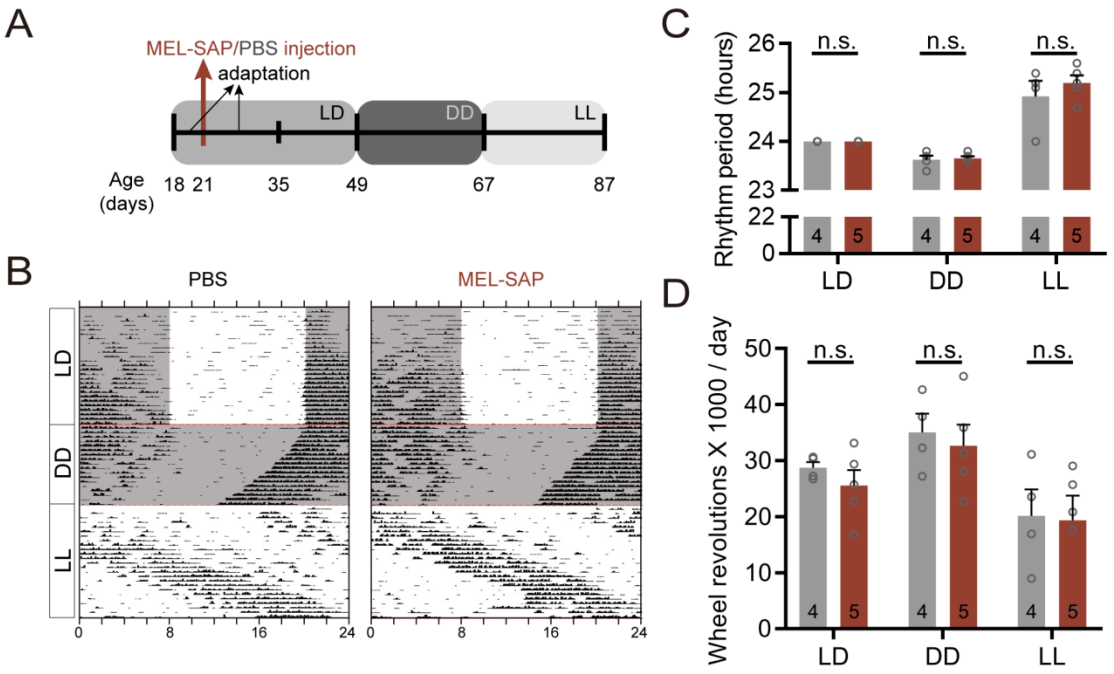

Fig. S2. Monocular ipRGC ablation does not affect circadian rhythm regulations. **(A)** Experimental timeline of intravitreal injections and wheel-running activity recordings of C57BL/6 mice under three lighting paradigms: 12: 12 h LD cycle (LD), constant darkness (DD) and constant light (LL). **(B)** Representative actograms recorded from a mouse with left eye injected with 400 ng MEL-SAP and another mouse with left eye injected with PBS (in both mice right eyes were injected with PBS). Each row represents a 24-h day. White and grey backgrounds indicate light and dark periods, respectively. **(C)** – **(D)** Bar graphs comparing circadian rhythm periods **(C)** and total wheel revolutions performed per day **(D)** between monocular ipRGC-ablated mice and control mice. For either parameter, no significant difference was detected between the two groups under any of the three lighting paradigms. Error bars represent SEM. n.s. not significant.

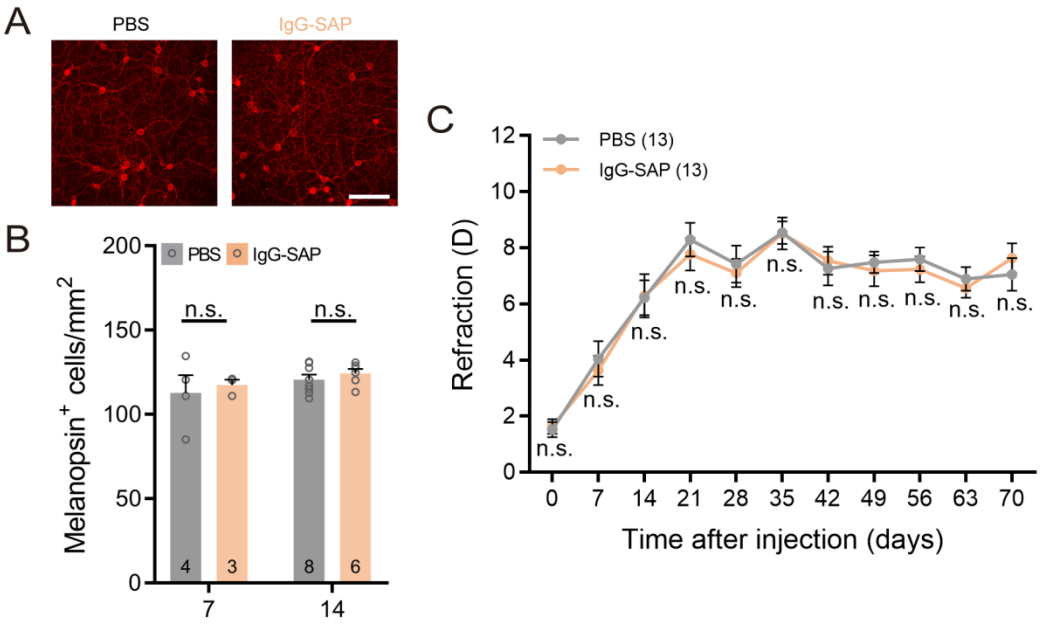

Fig. S3. IgG-SAP neither causes ipRGC death nor changes refractive development. **(A)** Representative micrographs of C57BL/6 retinal whole mounts stained with melanopsin, which were harvested at D14 from eyes injected with 400 ng IgG-SAP or PBS. Scale bar, 100 μm. **(B)** Bar charts summarizing melanopsin$^+$ cell densities in 400 ng IgG-SAP- and PBS-injected eyes at D7 and D14. At both time points, melanopsin$^+$ cell densities were indistinguishable between two eyes. **(C)** Comparison of refractive development between 400 ng IgG-SAP-injected and PBS-injected fellow eyes revealed no significant difference at any post-injection points. Error bars represent SEM. n.s. not significant.

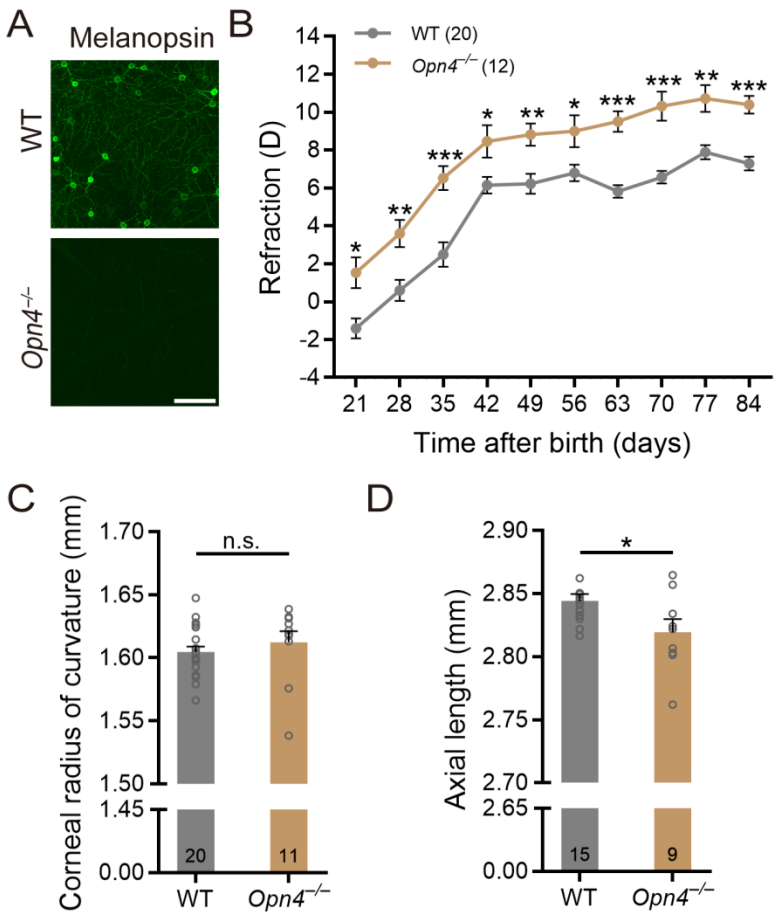

Fig. S4. Another melanopsin knockout mouse (*Opn4*$^{-/-}$) also shows hyperopic refractive shifts, along with shorter AL, as compared to wildtype littermates. (A) Immunohistochemistry using the UF008 antibody revealed no detectable melanopsin labeling in *Opn4*$^{-/-}$ retinas, whereas abundant melanopsin^{+} cells were found in retinas collected from breed-matched WT mice. Scale bar, 100 μm. **(B)** Growth curves of refractive errors in *Opn4*$^{-/-}$ and WT mice from P21 to P84. Note that at all sampling time points, *Opn4*$^{-/-}$ mice were significantly more hyperopic than WTs. **(C)** – **(D)** Bar charts comparing ocular biometry parameters measured at P84. The CRC was comparable between the two groups, whereas the AL of *Opn4*$^{-/-}$ mice was significantly smaller than that of WTs. Error bars represent SEM. n.s. not significant, * $P < 0.05$, ** $P < 0.01$, *** $P < 0.001$.

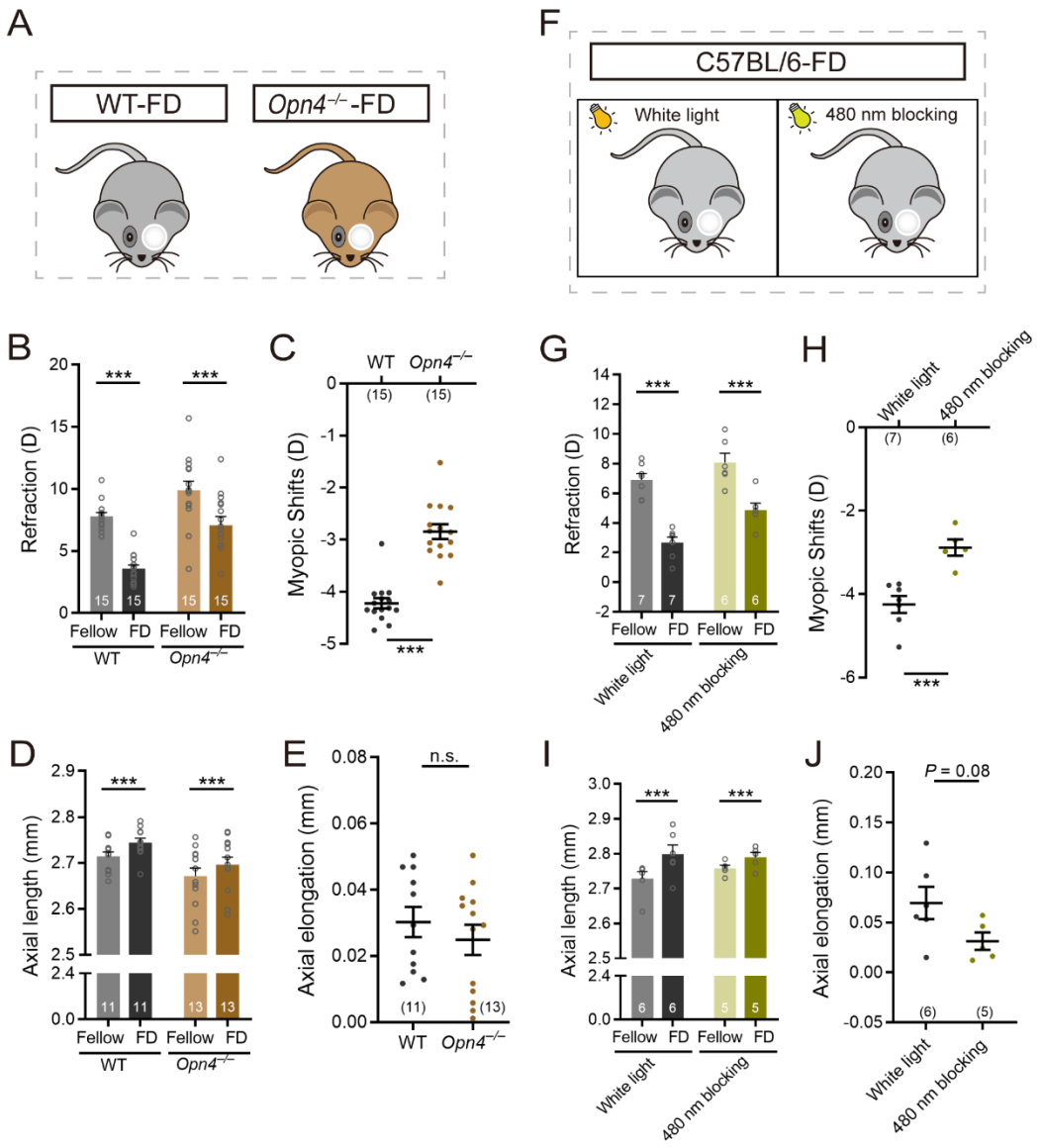

Fig. S5. Both *Opn4*$^{-/-}$ mice and 480 nm-blocking light-housed C57BL/6 mice show attenuated FDM. (A) Schematic illustration of wild-type (WT, *left*) and *Opn4*$^{-/-}$ mice (*right*); starting at P35, mice were form-deprived on left eyes for 4 weeks. **(B)** Form deprivation induced significant myopic shift in both *Opn4*$^{-/-}$ and breed-matched WT mice. **(C)** The myopic shifts induced in *Opn4*$^{-/-}$ mice were significantly smaller than those in WTs. **(D)** In both genotypes, the AL of deprived eyes, measured after 4-week form deprivation, was significantly larger than that of fellow eyes. **(E)** The form deprivation-induced axial elongation in *Opn4*$^{-/-}$ mice showed a trend of being smaller as compared with that in WT mice, but this trend did not reach statistical significance. **(F)** – **(J)** Same format as **(A)** – **(E)**, but for from-deprived C57BL/6 mice housed under white light and a 480 nm-blocking lighting environment. The latter environment was created by imposing a notch filter (~460 nm–500 nm band stop) to the white light source, which

attenuated the photon fluxes measured at 360 nm [λ_{max} of S (UV)-opsin], 480 nm (λ_{max} of melanopsin), 500 nm (λ_{max} of rhodopsin) and 510 nm (λ_{max} of M-opsin) by ~15%, ~91%, ~94% and ~36%, respectively. The residual intensity at 480 nm is ~1.7×10^{10} photons/cm^2/s, which hardly drives melanopsin-based ipRGC activity. The residual intensities sampled at 500 nm and 510 nm are ~2.6×10^{10} photons/cm^2/s and ~3.9×10^{11} photons/cm^2/s, respectively, well above the thresholds for rod and cone activation. Overall, under this 480 nm-blocking environment, the impairment of melanopsin signals may be, at least in part, responsible for the reduced myopic shifts. Error bars represent SEM. n.s. not significant, *** $P < 0.001$.

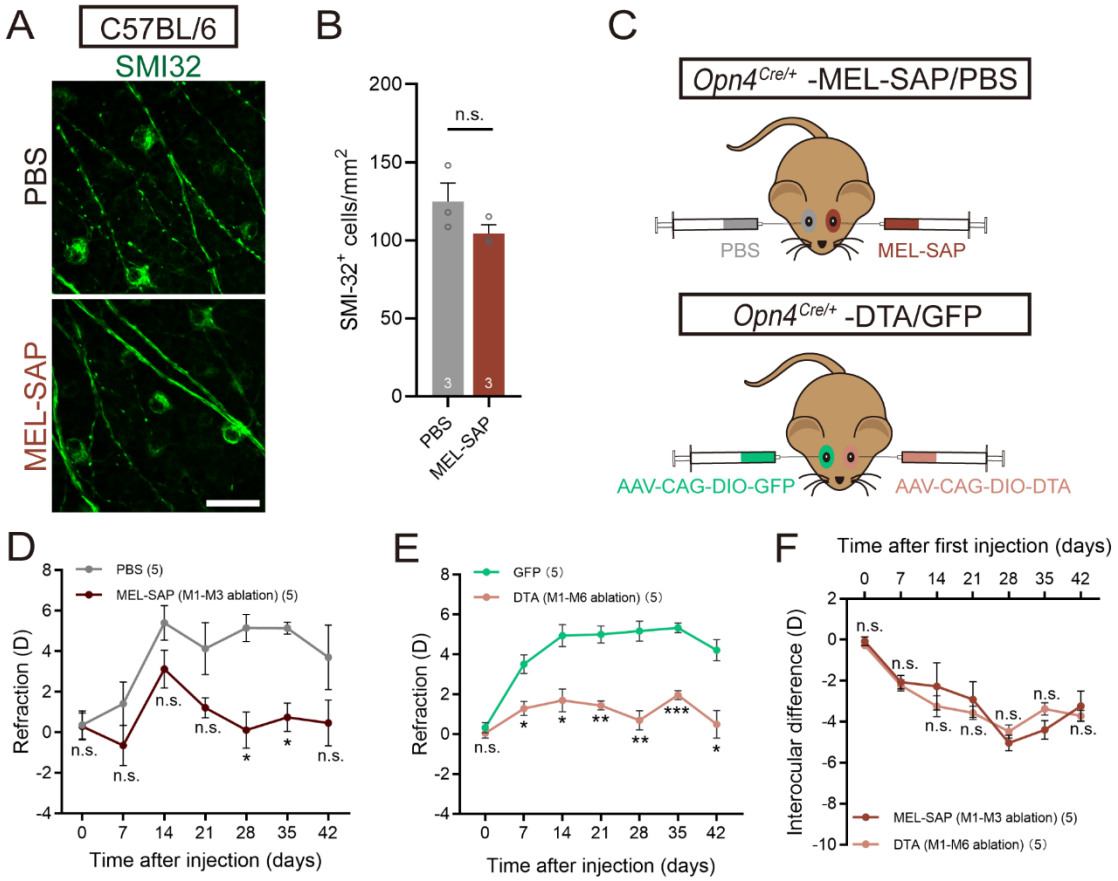

Fig. S6. M1–M3 cell-preferred ablation and M1–M6 cell uniform ablation result in myopic refractive shifts of similar magnitude. (A) – **(B)** Representative confocal images **(A)** and grouped data **(B)** showing unchanged densities of cells labeled by SMI-32, a marker for M4 cells, in 400 ng MEL-SAP-treated C57BL/6 retinas. Scale bar, 50 μm. **(C)** Schematic illustration of intravitreal injection of 400 ng MEL-SAP (preferentially ablating M1–M3 cells) or AAV-CAG-DIO-DTA (unbiasly ablating M1–M6 cells) in *Opn4*$^{Cre/+}$ mice. Fellow eyes were injected with PBS and AAV-CAG-DIO-GFP (control virus), respectively. **(D)** – **(E)** Both MEL-SAP- **(D)** and DTA-injected **(E)** eyes showed a significant myopic refractive shift relative to fellow eyes. **(F)** The magnitudes of myopic shift across ages are highly comparable between MEL-SAP- and DTA-injected eyes. n.s. not significant, * $P < 0.05$, ** $P < 0.01$, *** $P < 0.001$.

Table S1. Effects of MEL-SAP and form deprivation (FD) on ocular dimensions in C57BL/6 mice (Mean ± SEM, mm).

Group	Eye	Days after injection	n (n_{CRC})	CRC	CT	ACD	LT	VCD	RT	AL
MEL-SAP	Left (MEL-SAP)	70	12 (16)	1.572±0.014**	0.117±0.002	0.458±0.006*	1.638±0.004***	0.585±0.007	0.258±0.006	2.798±0.009**
	Right (PBS)			1.615±0.012	0.114±0.003	0.440±0.007	1.697±0.013	0.592±0.010	0.249±0.005	2.845±0.010
MEL-SAP	Left (MEL-SAP)	35	13 (13)	1.494±0.008***	0.117±0.003	0.422±0.006*	1.528±0.009***	0.659±0.008	0.235±0.006	2.726±0.009**
	Right (PBS)			1.569±0.012	0.109±0.003	0.406±0.005	1.585±0.004	0.667±0.006	0.221±0.006	2.767±0.008
MEL-SAP + FD	Left (MEL-SAP + FD)	35	10 (11)	1.483±0.007	0.106±0.003	0.460±0.007	1.505±0.006	0.652±0.007*	0.235±0.008	2.723±0.009**
	Right (MEL-SAP)			1.487±0.008	0.113±0.004	0.455±0.012	1.505±0.012	0.628±0.009	0.250±0.005	2.701±0.011
PBS + FD	Left (PBS + FD)	35	10 (11)	1.567±0.010	0.105±0.002	0.452±0.010	1.593±0.010	0.655±0.007	0.230±0.005	2.805±0.008***
	Right (PBS)			1.572±0.009	0.100±0.003	0.445±0.007	1.590±0.008	0.634±0.008	0.238±0.004	2.760±0.0110

* $P < 0.05$, ** $P < 0.01$, *** $P < 0.001$, paired *t*-test, Left vs Right eyes. CRC, corneal radius of curvature; CT, corneal thickness; ACD, anterior chamber depth; LT, lens thickness; VCD, vitreous chamber depth; RT, retinal thickness; AL, axial length; n_{CRC}, sample number of CRC measurements.

Table S2. Effects of selective chemogenetic activation of ipRGCs and targeted M1 cell ablation on ocular dimensions in *Opn4*$^{Cre/+}$ mice (Mean ± SEM, mm).

Group	Eye	Weeks	n (n_{CRC})	CRC	CT	ACD	LT	VCD	RT	AL
Opn4$^{Cre/+}$	Left (hM3Dq)	9	10 (10)	1.584±0.006*	0.104±0.002	0.398±0.006	1.680±0.021	0.598±0.020	0.243±0.006	2.780±0.011*
	Right (GFP)			1.569±0.007	0.101±0.003	0.408±0.011	1.648±0.015	0.595±0.010	0.252±0.003	2.753±0.010
Opn4$^{Cre/+}$	Left (Flp + fDIO-DTA)	9	8 (8)	1.519±0.010*	0.088±0.003	0.367±0.007	1.680±0.011	0.633±0.011	0.269±0.004	2.768±0.015
	Right (mCherry + fDIO-DTA)			1.542±0.013	0.096±0.004	0.389±0.027	1.653±0.018	0.623±0.022	0.278±0.007	2.761±0.008

* $P < 0.05$, paired *t*-test, Left vs Right eyes. CRC, corneal radius of curvature; CT, corneal thickness; ACD, anterior chamber depth; LT, lens thickness; VCD, vitreous chamber depth; RT, retinal thickness; AL, axial length; n_{CRC}, sample number of CRC measurements.

Table S3. Summary of ocular dimensions in *Opn4*$^{Cre/Cre}$ mice with different treatments (Mean ± SEM, mm).

Group	Eye	Weeks after birth	n (n_{CRC})	CRC	CT	ACD	LT	VCD	RT	AL
Opn4$^{Cre/Cre}$	Left and Right	9	12 (14)	1.583±0.007	0.099±0.003	0.389±0.008	1.615±0.010	0.594±0.006	0.246±0.004	2.696±0.008$^{\#}$
WT	Left and Right	9	12 (15)	1.573±0.005	0.102±0.002	0.393±0.004	1.631±0.005	0.600±0.005	0.243±0.004	2.725±0.009
Opn4$^{Cre/Cre}$-DTA	Left (DTA)	9	13 (17)	1.543±0.004***	0.101±0.001	0.392±0.007	1.607±0.012	0.601±0.004	0.245±0.005	2.702±0.013
	Right (GFP)			1.586±0.006	0.100±0.003	0.391±0.008	1.593±0.019	0.611±0.008	0.235±0.003	2.694±0.016
Opn4$^{Cre/Cre}$-FD	Left (FD)	9	16 (16)	1.566±0.004	0.096±0.002	0.371±0.005	1.607±0.007	0.608±0.005	0.248±0.005	2.682±0.007***
	Right (Fellow)			1.565±0.004	0.096±0.002	0.363±0.006	1.607±0.008	0.599±0.006	0.247±0.004	2.666±0.008
WT-FD	Left (FD)	9	12 (12)	1.564±0.004	0.097±0.004	0.388±0.006**	1.627±0.008	0.615±0.008*	0.246±0.008	2.727±0.008***
	Right (Fellow)			1.563±0.003	0.097±0.003	0.374±0.005	1.622±0.008	0.601±0.007	0.244±0.003	2.694±0.007
Opn4$^{Cre/Cre}$-DTA + FD	Left (DTA + FD)	9	10 (13)	1.528±0.005	0.098±0.003	0.382±0.007	1.590±0.009	0.618±0.009	0.244±0.007	2.688±0.011**
	Right (DTA + Fellow)			1.530±0.004	0.099±0.002	0.378±0.004	1.586±0.012	0.613±0.010	0.244±0.005	2.676±0.010
Opn4$^{Cre/Cre}$-GFP + FD	Left (GFP + FD)	9	10 (10)	1.572±0.004	0.099±0.003	0.381±0.006	1.607±0.006	0.606±0.006	0.240±0.003	2.693±0.010***
	Right (GFP + Fellow)			1.576±0.003	0.097±0.002	0.378±0.010	1.615±0.007	0.587±0.010	0.244±0.004	2.678±0.009

$^{\#}$ $P < 0.05$, unpaired *t*-test, *Opn4*$^{Cre/Cre}$ mice vs WT mice. * $P < 0.05$, ** $P < 0.01$, *** $P < 0.001$, paired *t*-test, Left vs Right eyes. CRC, corneal radius of curvature; CT, corneal thickness; ACD, anterior chamber depth; LT, lens thickness; VCD, vitreous chamber depth; RT, retinal thickness; AL, axial length; n_{CRC}, sample number of CRC measurements; FD, form deprivation.

Table S4. Summary of ocular dimensions in DD- and LD-raised *rd/rd cl* mice (Mean ± SEM, mm).

Group	Eye	Weeks	n (n_{CRC})	CRC	CT	ACD	LT	VCD	RT	AL
rd/rd cl (DD)	Left + Right	7	11 (15)	1.539±0.003	0.098±0.002	0.381±0.007	1.543±0.011	0.658±0.015	0.153±0.005	2.681±0.009$^{\#\#}$
rd/rd cl (LD)	Left + Right		13 (13)	1.541±0.006	0.094±0.002	0.392±0.010	1.538±0.007	0.699±0.014	0.159±0.007	2.722±0.010

$^{\#\#}$ $P < 0.01$, unpaired *t*-test, DD vs LD. CRC, corneal radius of curvature; CT, corneal thickness; ACD, anterior chamber depth; LT, lens thickness; VCD, vitreous chamber depth; RT, retinal thickness; AL, axial length; n_{CRC}, sample number of CRC measurements.